

Investigation of Sm → Ca substitution in Bi(Pb)SrCaCuO high temperature superconductor by low field AC magnetic susceptibility

Cabir Terzioglu · Dincer Yegen · Mustafa Yilmazlar ·
Osman Gorur · Mustafa Akdogan · Ahmet Varilci

Received: 6 January 2006 / Accepted: 6 June 2006 / Published online: 16 February 2007
© Springer Science+Business Media, LLC 2007

Abstract We have investigated the effect of Sm substitution in Bi(Pb)SrCaCuO system by performing AC susceptibility ($\chi = \chi' + i\chi''$), XRD (X Ray Diffraction) and SEM (Scanning Electron Microscopy) measurements. The Sm → Ca substitution ($\text{Bi}_{1.6}\text{Pb}_{0.4}\text{Sr}_2\text{Ca}_{2-x}\text{Sm}_x\text{Cu}_3\text{O}_y$) was carried out by conventional solid-state reaction method. The susceptibility measurements were carried out at different values of the AC field amplitudes. The imaginary part of susceptibility is used to estimate the intergranular critical current density by means of the Bean's model. The intergranular critical current density (J_c) of pure sample is found to be about 68 A/cm² at 95 K. The intergranular J_c is seen to decrease with increasing Sm substitution. XRD pattern and SEM micrographs are given to provide information about Bi-2223 phase and grain size respectively.

Introduction

In order to find out new materials with critical temperatures higher than the liquid nitrogen temperature,

the researchers have substituted various rare-earth ions in the Bi(Pb)SrCaCuO system. XRD, electrical resistance, AC susceptibility and DC magnetization techniques are frequently used to investigate the superconducting properties of the $\text{Bi}_2\text{Sr}_2\text{Ca}_{2-x}\text{Sm}_x\text{Cu}_3\text{O}_y$ system [1, 2]. The substitution of Sm^{3+} (mean ionic size is 0.96 Å) for Ca^{2+} (mean ionic size is 0.99 Å) is found to change the superconducting properties of the BiSr(Pb)CaCuO system. The results show that the $\text{Sm}^{3+} \rightarrow \text{Ca}^{2+}$ substitution changes the hole carrier concentration, which in turn lowers T_c^{off} (offset, $\rho = 0$) and decreases the volume fraction of the superconducting phase [3]. The transport and magnetic critical current density in BSCCO system also depends on oxygen content [4]. The AC susceptibility is the most convenient measuring method using the mutual inductance principle [5]. It is used extensively to study spin glass phenomena, superconducting transitions, vortex dynamics and critical current densities and to map magnetic phase diagrams. In this method, applied field is very small, so the magnetic ground state is probed. Dynamic magnetic and superconducting phenomena can be measured directly usually over a frequency range of 10 Hz to 100 kHz. The AC susceptibility measurements ($\chi = \chi' + i\chi''$) are often used to reveal the superconducting properties of BiSrCaCuO system [6]. The sharp decrease in the real part χ' (T) below the critical temperature T_c^{on} (onset) is a manifestation of diamagnetic shielding and the peak in the imaginary part χ'' (T) represents the AC losses [7]. The AC susceptibility data strongly depend on the AC magnetic field amplitude and slightly on the AC frequency. Considerable frequency dependence has not been observed in the low frequency range below 10 kHz [8, 9]. At large AC field amplitudes (typically

C. Terzioglu · D. Yegen · M. Akdogan · A. Varilci (✉)
Faculty of Arts and Sciences, Department of Physics,
Abant Izzet Baysal University, Bolu 14280, Turkey
e-mail: varilci_a@ibu.edu.tr

M. Yilmazlar
Faculty of Arts and Sciences, Department of Physics,
Kirikkale University, Kirikkale 71450, Turkey

O. Gorur
Rize Faculty of Arts and Sciences, Department of Physics,
Karadeniz Technical University, Rize 53100, Turkey

greater than 5 Oe) often two loss peaks are found [10]. It is well known that the critical current density is one of the most important parameters of superconductors in their wide ranging applications. The critical current is essentially determined by the flux pinning mechanism. When the flux lines fully penetrate the material, i.e., when H_{applied} is equal to the first full penetration field H_* , the losses reach a maximum [11, 12]. Using this fact, one can calculate the critical current density as a function of temperature using the critical state model [13, 14].

In this communication, we present $\chi(T)$, XRD and SEM measurements of Sm substituted Bi(Pb)SrCaCuO samples prepared by the solid-state method. Changes in T_c and J_c (intergranular critical current density) by increasing Sm concentration are explained on the basis of granular superconductivity. We give detailed results of the low field AC susceptibility studies and calculation of intergranular J_c values in the Sm (in place of Ca) substituted Bi-2223 samples.

Experimental

For the synthesis of $\text{Bi}_{1.6}\text{Pb}_{0.4}\text{Sr}_2\text{Ca}_{2-x}\text{Sm}_x\text{Cu}_3\text{O}_y$ ($x = 0.0, 0.0005, 0.001, 0.005, 0.01, 0.05, 0.1, 0.5, 1$ and 1.5), the samples were prepared from Bi_2O_3 , PbO , SrCO_3 , CaO , Sm_2O_3 and CuO , taken in stoichiometric proportions by the standard solid-state reaction methods. The samples prepared with $x = 0.01, 0.05, 0.1, 0.5, 1$ and 1.5 values were not superconducting at 77 K. For this reasons, only the samples with $x = 0.0, 0.0005, 0.001$ and 0.005 values are investigated in this work since studied over liquid nitrogen temperature. For isothermal annealing of the samples with different Sm amount, seven different mixtures are calcinated at 800 °C for 24 h simultaneously. After the treatment, the mixtures was reground, pressed into pellets 13 mm in diameter, then annealed at 860 °C for 200 h under similar conditions. The heating and cooling rates of the tube furnace for annealing were chosen to be 5 and 3 °C/min, respectively. After cooling to room temperature, the pellets were cut into rectangular bar shape ($0.97 \times 2.42 \times 8.12 \text{ mm}^3$) for the AC susceptibility measurements.

AC susceptibility measurements on the samples were made using a home-made AC susceptometer and a Lock-in Amplifier (Stanford Research SR850). The susceptometer consists of two identical secondary coils within the primary coil. The sample was mounted with vacuum grease tightly on the sample holder at the centre of one of the secondaries. The temperature measurement was carried out by Cu-Constantan

thermocouple attached to the sample. The uncertainty of temperature measurements is about 20 mK. The AC field was applied along the longest dimension of the samples. The coil system was placed in a vacuum sealed pyrex tube, which was then evacuated by a vacuum pump and He gas is transferred into the tube as an exchange gas. He gas pressure was about 1 bar. Afterwards, pyrex tube inserted into the liquid nitrogen bath. The measurements started at 77 K with heating rate of 2 K/min in the temperature range 77–110 K at AC field amplitudes of 111, 222, 333, 444 and 555 A/m and at 1 kHz frequency. Susceptibility data taken from Lock-in Amplifier were recorded using the Labview computer programme. The values of intergranular critical current densities $J_c(T_p)$ in our samples were calculated using the Bean's model from the acquired data. The estimates of the average grain size in the samples were made through scanning electron micrographs (SEM). SEM magnification is 1,800.

Phase purity and the lattice parameters were determined by XRD. XRD data were taken using a Rigaku D/Max-IIIIC diffractometer with CuK_α radiation in the range $2\theta = 4^\circ\text{--}60^\circ$ with a scan speed of $3^\circ/\text{min}$ and a step increment of 0.02° . The accuracy in determining the lattice parameter c was $\pm 0.001 \text{ \AA}$. The mean values of c lattice parameters of pure and Sm substituted Bi(Pb)SrCaCuO samples determined from the high-angle (00 l) peaks of the XRD measurements (Table 1).

Results and discussion

Figure 1 displays the AC susceptibility (χ' and χ'') versus temperature plots for pure and Sm substituted $\text{Bi}_{1.6}\text{Pb}_{0.4}\text{Sr}_2\text{Ca}_{2-x}\text{Sm}_x\text{Cu}_3\text{O}_y$ samples ($x = 0.0005, 0.001$ and 0.005). The real part of the susceptibility (in-phase component) is normalized to -1 to compare the samples substituted with different Sm amount. The real parts of susceptibility for the pure sample (Fig. 1a) starts to drop down at $T_c^{\text{on}}=102 \text{ K}$ (termed as onset of bulk superconductivity) with decreasing temperature for different magnetic field values. They exhibit field independent behaviour until 98 K, below which they diverge. This temperature is the increasing point of the imaginary part (out of phase component). Imaginary parts show peaks at 97, 96, 95, 94 and 93 K for the fields 111, 222, 333, 444 and 555 A/m respectively. As seen from the figure, maximum peak temperature of imaginary part (T_p) shifts to left when the field amplitude increases. The shift may be attributed to the strength of the pinning force. The weaker the pinning, the larger is the shift in the

Table 1 Some characteristics of superconducting samples

Sample	f_g (volume fraction of grains)	Lattice Parameter c (Å)	T_c^{on} (K)	T_p (K) (for 111 A/m)	Transport J_c (A/cm ²) at 77.4 K
Pure	0.068	37.236	102	97	43
$x = 0.0005$	0.021	37.206	101	88	38
$x = 0.001$	0.017	37.197	99	86	32
$x = 0.005$	0.007	37.190	99	85	8

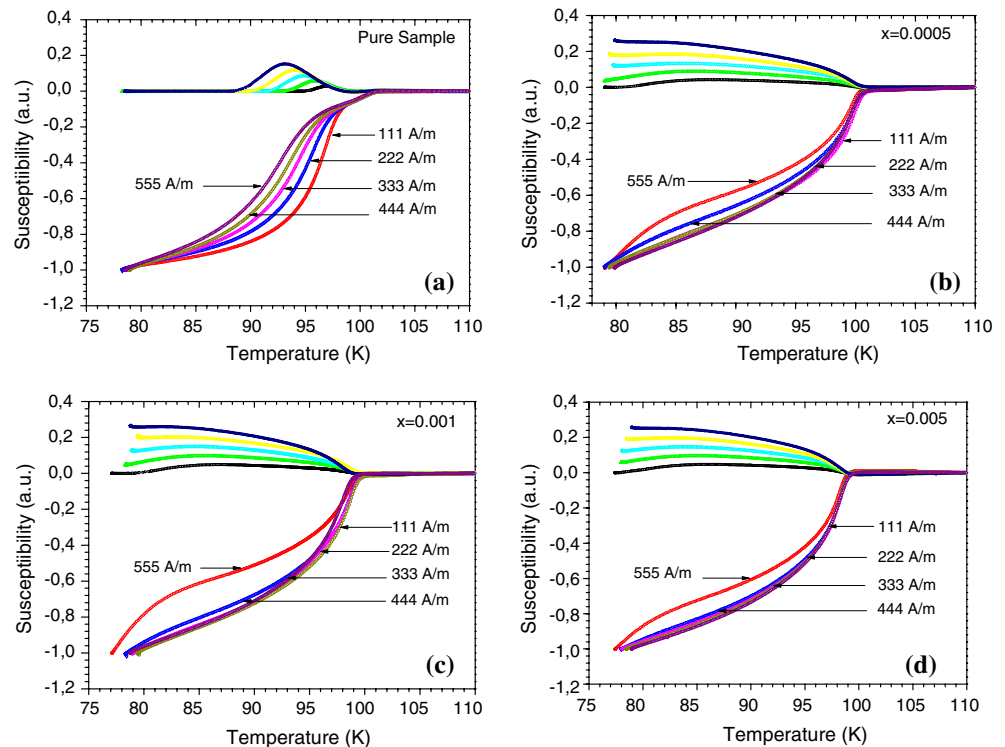
maximum of χ'' [15]. At the peak values of the imaginary part, AC field amplitude equals to the full flux penetration field, H_p . At large AC field amplitudes (typically greater than 400 A/m) often two loss peaks are found; a broad peak at low temperature (coupling losses) and a narrower peak (intrinsic losses) near T_c^{on} . We did not see any intrinsic loss peaks in our samples. This may be due to small inter-granular potential, small grain size and no flux penetration into the grains of the sample [2, 10].

It can be seen in Fig. 1(b–d) that Sm substitution shifts the susceptibility-temperature curves to lower temperature side and considerably increases the transition width in χ'' - T curves and also decreases the shielding fraction of the superconducting phase in the samples. This is explained with details in the literature [13, 14]. In view of that, the broadening of the peak with increasing Sm substitution is due to gradual penetration of flux into the centre of the intergranular regions. The real and imaginary parts are zero ($\chi' = \chi'' = 0$) when the sample is in normal state (full

penetration). χ'' turns positive due to the extent of increasing flux penetration as the temperature shows slight decrease below T_c^{on} . At T_p , full penetration is realized and peak reaches its maximum. The amplitude of χ'' falls due to decreasing amount of flux penetration, below T_p . When the temperature reaches to lowest value ($\chi = -1$ and $\chi'' = 0$) the whole body starts to shield. This is apparent indication of the destructive effect in the superconducting properties brought about by Sm–Ca replacement in the Bi-2223 system. This is in line with previous work [16].

We estimated the temperature dependence of intergranular J_c using the Bean's model [17]. Accordingly, when flux lines fully penetrate to the sample, losses reaches to highest value. The intergranular J_c is calculated in our sample using the relation $J_c(T_p) = H_a/a$ for the sample having cross section of the rectangular bar shaped sample, like $2a \times 2b$ where $a < b$ [18]. H_a is the amplitude of applied field at T_p . According the Bean model, imaginary part of the AC susceptibility for cylindrical geometry can be written as

Fig. 1 AC susceptibility ($\chi = \chi' + i\chi'' = 0$) versus temperature plots for Bi_{1.6}Pb_{0.4}Sr₂Ca_{2-x}Sm_xCu₃O_y samples with different amount of Sm substitution ($x = 0.0, 0.0005, 0.001$ and 0.005)



$$\chi'' = \left[\left(4 \frac{H_{\text{applied}}}{H_a} \right) - 2 \left(\frac{H_{\text{applied}}}{H_a} \right)^2 \right] \frac{1}{3\pi}, \text{ for } H_a \geq H_{\text{applied}}$$

$$\chi'' = \left[\left(4 \frac{H_{\text{applied}}}{H_a} \right) - 2 \left(\frac{H_{\text{applied}}}{H_a} \right)^2 \right] \frac{1}{3\pi}, \text{ for } H_a \leq H_{\text{applied}}$$

Figure 2 shows the Cole–Cole plots of the first harmonics for the different Sm substituted samples. The samples are measured at $H_a = 111 \text{ A/m}$ and $f = 1 \text{ kHz}$. The volume fraction of grains, f_g , for each sample (see Table 1) can be estimated from the graph. f_g decreases with increasing amount of Sm substitution. Chen et al. [19] used the critical state model of Kim et al. [20] to calculate AC susceptibility and determined the volume fraction of the grains for Bi(Pb)SrCaCuO superconductors. The determined f_g value also used by Celebi [7] to calculate the matrix susceptibility. The Cole–Cole plots are characterized by the dome and triangle shaped curve with maximum that rises if H_{applied} is increased. The occupied area of the $\chi''(\chi')$ graph for the pure sample at 111 A/m is about 1/3 less than that of the $x = 0.0005$ Sm substituted sample.

Resistivity versus temperature graph is given in Fig. 3. The resistivity of pure sample at 140 K is significantly lower than the Sm substituted samples. The offset critical temperature (T_{offset}) of Bi(Pb)SrCaCuO sample decreases as the Sm amount increases. The Sm amount with $x = 0.01$ suddenly lowers T_{offset} of the sample with $x = 0.005$ from 92 to 72 K. The Sm substitution with $x = 0.1$ was detrimental for supercon-

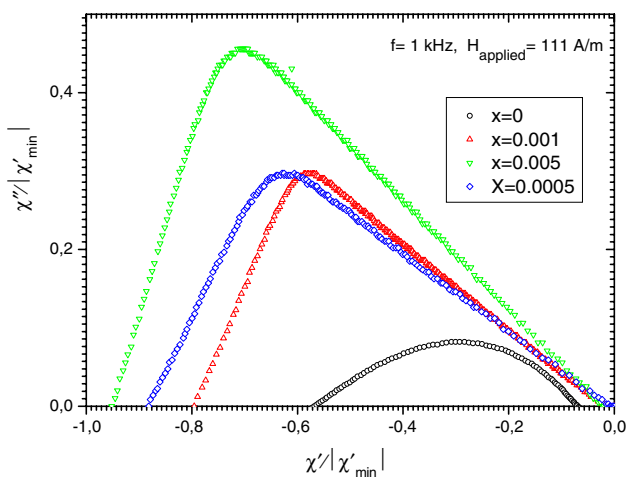


Fig. 2 Plot of χ'' versus χ' components of AC magnetic susceptibility behavior at 1 kHz and $H_{\text{applied}} = 111 \text{ A/m}$ for samples with different x values

ductivity. This superconductivity damage by Sm substitution was reported before [20, 21].

Figure 4 exhibits the intergranular critical current (J_c) density versus temperature for the pure and Sm substituted samples. As seen from the graph, J_c is about 68 A/cm^2 for pure Bi(Pb)SrCaCuO sample at 95 K. At 85 K, the critical current density decreases as 37, 28 and 24 A/cm^2 for the samples with $x = 0.0005, 0.001$ and 0.005 , respectively.

Transport critical current density is also measured for these samples at liquid nitrogen temperature. It is seen from Table 1 that the Sm substitution brings out an reduction in the J_c of the Bi(Pb)SrCaCuO sample. The lower J_c in comparison with increasing Sm concentration may ascribe to a very weak link.

The XRD patterns of pure, $x = 0.01$ and 0.1 Sm substituted samples are shown in Fig. 5. There is significant increase in the intensities of $(hkl)H$ peaks between the pure and $x = 0.01$ Sm substituted samples. $(hkl)H$ peaks at $x = 0.01$ sample turn to $(hkl)L$ peaks at $x = 0.1$ Sm substituted samples. The determined lattice parameters c from the $(00l)$ peaks of the XRD data are given in Table 1. It is observed that the lattice parameter c decreases significantly with increasing Sm content as listed in Table 1. Similar result has been reported by Zandbergen et al. [22]. As pointed out by Zandbergen et al. the behaviour of the lattice parameter can be explained by the increase of the oxygen content in the unit cell by the replacement of Ca^{+2} by Sm^{+3} in the structure. It was speculated that the excess of oxygen goes into the bismuth oxide layers causing a decrease in parameter c . It is also believed that the decrease of parameter c is due to incorporation of Sm ions into the interstitial sites in the unit cell rather than occupation of the Ca sites.

Figure 6 represents the SEM micrographs of $x = 0$ and $x = 0.005$ Sm substituted Bi(Pb)SrCaCuO samples. The grain density of pure sample is relatively higher than that of the Sm substituted Bi(Pb)SrCaCuO samples. It may be said that Sm substituted sample has comparatively denser surface structure. The relatively low intergranular J_c for Sm substituted samples (Fig. 4) with respect to the undoped sample may be attributed to have lower grain density.

Conclusions

The $\text{Sm} \rightarrow \text{Ca}$ substitution in Bi(Pb)SrCaCuO system decreased the intergranular J_c of the sample with $x = 0.0005, 0.001$ and 0.005 . T_p is shifted with increasing applied magnetic field. Broadening of the peak is also observed. This is ascribed to weak pinning and

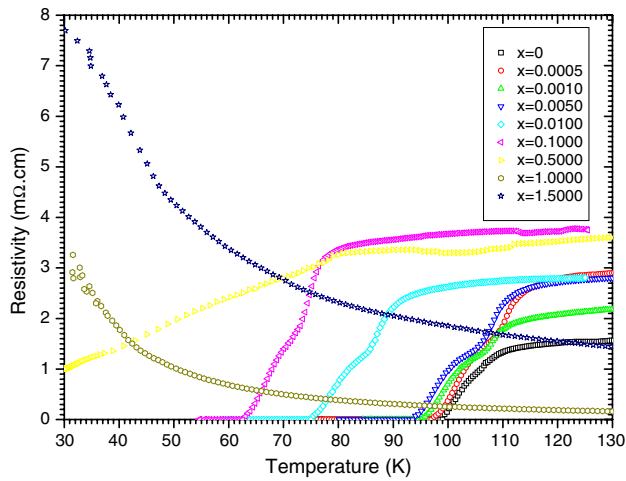


Fig. 3 The resistivity versus temperature plots for the $\text{Bi}_{1.6}\text{Pb}_{0.4}\text{Sr}_2\text{Ca}_{2-x}\text{Sm}_x\text{Cu}_3\text{O}_y$ ($x = 0.0, 0.0005, 0.001, 0.005, 0.01, 0.1, 0.5, 1$ and 1.5) samples

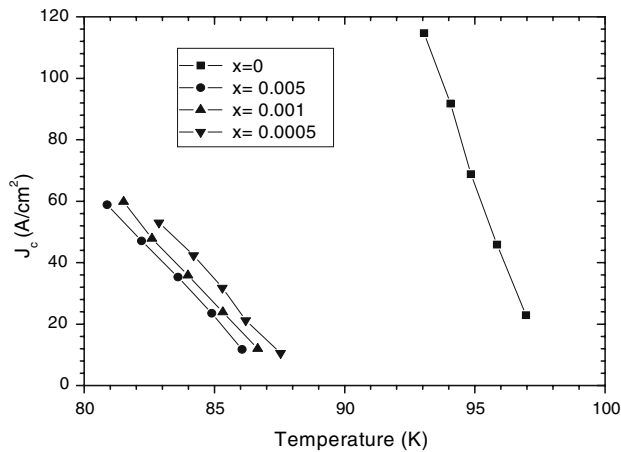


Fig. 4 The intergranular critical current density versus temperature plots for the $\text{Bi}_{1.6}\text{Pb}_{0.4}\text{Sr}_2\text{Ca}_{2-x}\text{Sm}_x\text{Cu}_3\text{O}_y$ ($x = 0.0, 0.0005, 0.001$ and 0.005) samples. Solid lines are drawn for eye-guide only

relatively small intergranular J_c . It is found that volume fractions of grains, estimated from Cole–Cole plot of AC susceptibility data, decrease with increasing amount of Sm substitution. AC matrix susceptibility data has been calculated from the volume fractions of grains. The lattice parameter c calculated using XRD patterns decreased with increasing amount of Sm substitution. On the other hand, small changes in grain sizes and grain boundary conditions may be seen from SEM micrographs for the pure and Sm substituted sample. There are not much changes in T_c^{on} with small ($x = 0.0005, 0.001$ and 0.005) $\text{Sm} \rightarrow \text{Ca}$ substitution in $\text{Bi}(\text{Pb})\text{SrCaCuO}$ system. Also superconductivity is not observed for the samples $x = 0.01, 0.05$ and 0.1 at 77 K.

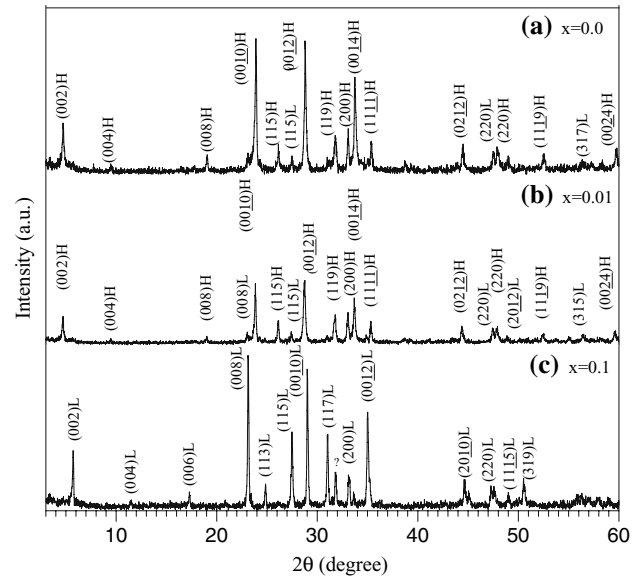


Fig. 5 The XRD patterns for (a) pure sample, (b) $x = 0.01$ and (c) $x = 0.1$ Sm substituted sample. Peaks of the high- T_c and Low- T_c phases are indexed H and L, respectively

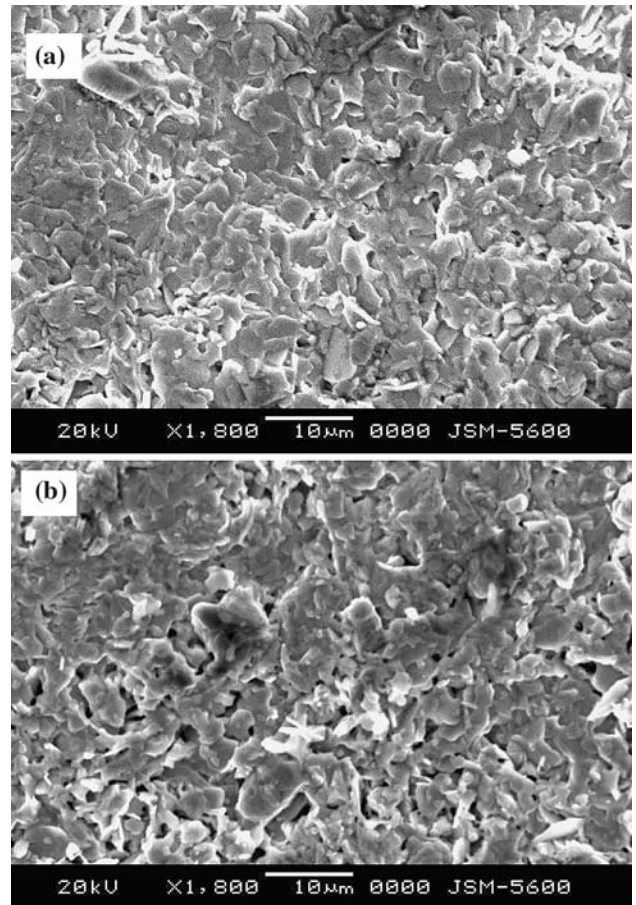


Fig. 6 SEM micrographs of (a) pure and (b) $x = 0.005$ Sm substituted $\text{Bi}(\text{Pb})\text{SrCaCuO}$ sample annealed at the same conditions

References

1. Nanda KK, Satyavathi S, Muralithar M, Hari Babu V, Pena O (1994) *Physica C* 1519–1520:239
2. Goldfarb RB, Leirental M, Thomson CA (1991). In: Hein RA, Francavilla TL, Liebenberg DH (eds) *Magnetic susceptibility of superconductors and other spin systems*. Plenum Press, New York
3. Nanda KK, Muralidhar M, Hari Babu V, Pena O, Sergent M, Beniere F (1993) *Physica C* 229–304:204
4. Balestrino G, Livanov DV, Milani E, Camarota B, Fiorani D, Tesla AM (1994) *Phys Rev B* 50:5
5. Akune T, Abe H, Koga A, Sakamoto N, Matsumoto Y (2002) *Physica C* 234–238:378
6. Gencer A, Aksu E, Yilmaz H, Aydınuraz A (2002) *Supercond Sci Technol* 15:592
7. Celebi S (1999) *Physica C* 251–256:316
8. Malozemoff AP, Worthington TK, Yeshurun Y, Holtzberg F, Kes PH (1988) *Phys Rev B* 7203:38
9. Li JW, Wang RL, Yi HR, Li HC, Yin B, Li L (1992) *Phys Rev B* 9190:46
10. Muller KH, Collocott SJ, Driver R, Savvides N (1991) *Supercond Sci Technol* 325–327:4
11. Clem JR (1998) *Physica C* 50:153
12. Aksu E, Gencer A, Yilmaz H, Nezir S (2003) *Physica C* 67–74:391
13. Chen DX, Nogues J, Rao KV (1989) *Cryogenics* 800:29
14. Gomory F, Lobotka P (1988) *Solid State Commun* 645:66
15. Celebi S, Nezir S, Gencer A, Yanmaz E, Altunbas M (1997) *J Alloys Comp* 5–10:255
16. Coskun A, Ekicibil A, Ozcelik B, Kiyamac K (2004) *Chin Phys Lett* 20041:21
17. Bean CP (1964) *Rev Mod Phys* 31:36
18. Agarwal SK, Kumaraswamy BV (2005) *J Phys Chem Solids* 729–734:66
19. Chen DX, Mei Y, Luo HL (1990) *Physica C* 167:317
20. Kim YB, Hemstead CF, Strnad AR (1962) *Phys Rev Lett* 9:306
21. Nanda Kishore K, Muralidhar M, Hari Babu V, Peña O, M Sergent, Bénéière F (1993) *Physica C: Superconductivity* 204:3–4, 299–304
22. Zandbergen HW, Greon WA, Smit A, Tendeloo GV (1990) *Physica C* 168:426